Insights into the Dose–Response Relationship of Radioembolization with Resin ^{90}Y-Microspheres: A Prospective Cohort Study in Patients with Colorectal Cancer Liver Metastases

Andor F. van den Hoven[1], Charlotte E.N.M. Rosenbaum[1], Sjoerd G. Elias[1,2], Hugo W.A.M. de Jong[1], Miriam Koopman[3], Helena M. Verkooijen[1], Abass Alavi[4], Maurice A.A.J. van den Bosch[1], and Marnix G.E.H. Lam[1]

[1]Department of Radiology and Nuclear Medicine, University Medical Center Utrecht, Utrecht, The Netherlands; [2]Julius Center for Health Sciences and Primary Care, University Medical Center Utrecht, Utrecht, The Netherlands; [3]Department of Medical Oncology, University Medical Center Utrecht, Utrecht, The Netherlands; and [4]Division of Nuclear Medicine, Hospital of the University of Pennsylvania, Philadelphia, Pennsylvania

Randomized controlled trials are investigating the benefit of hepatic radioembolization added to systemic therapy in the first- and second-line treatment of patients with colorectal liver metastases (CRLM). Remarkably, administered activity may still be suboptimal, because a dose–response relationship has not been defined. The purpose of this study was to characterize the relationship between tumor-absorbed dose and response after ^{90}Y radioembolization treatment for CRLM. **Methods:** Thirty patients with unresectable chemorefractory CRLM were treated with resin ^{90}Y-microspheres in a prospective phase II clinical trial. Tumor-absorbed dose was quantified on ^{90}Y PET. Metabolic tumor activity, defined as tumor lesion glycolysis (TLG*) on ^{18}F-FDG PET, was measured at baseline and 1 mo after treatment. The relationship between tumor-absorbed dose and posttreatment metabolic activity was assessed per metastasis with a linear mixed-effects regression model. **Results:** Treated metastases (n = 133) were identified. The mean tumor-absorbed dose was 51 ± 28 Gy (range, 7–174 Gy). A 50% reduction in TLG* was achieved in 46% of metastases and in 11 of 30 (37%) patients for the sum of metastases. The latter was associated with a prolonged median overall survival (11.6 vs. 6.6 mo, P = 0.02). A strong and statistically significant dose–response relationship was found ($P < 0.001$). The dose effect depended on baseline TLG* ($P < 0.01$). The effective tumor-absorbed dose was conservatively estimated at a minimum of 40–60 Gy. **Conclusion:** A strong dose–response relationship exists for the treatment of CRLM with resin microsphere ^{90}Y radioembolization. Treatment efficacy is, however, still limited, because the currently used pretreatment activity calculation methods curb potentially achievable tumor-absorbed dose values. A more personalized approach to radioembolization is required before concluding on its clinical potential.

Key Words: radioembolization; ^{90}Y PET; dose-response relationship; metabolic tumor response; CRLM

J Nucl Med 2016; 57:1014–1019
DOI: 10.2967/jnumed.115.166942

Radioembolization has become an established treatment for patients with unresectable chemorefractory colorectal cancer liver metastases (CRLM). During this treatment, the hepatic arterial vasculature is catheterized, and radioactive microspheres are injected into the bloodstream. The preferential arterial vascularization of liver tumors induces selective clustering of ^{90}Y-microspheres around tumors, where they emit tumoricidal β-irradiation while relatively sparing healthy liver tissue (*1*).

A beneficial effect on liver disease control has already been shown in the salvage setting, and large randomized controlled trials are investigating the role of radioembolization with concomitant systemic therapy as first- or second-line treatment (*2,3*).

Prescribed activity calculations are currently not personalized. For resin ^{90}Y-microspheres, activity planning is based on the body surface area (BSA) method. This simple method was developed to calculate safe treatment activities, but it does not incorporate a target tumor-absorbed dose, nor does it account for interindividual differences in microspheres distribution. Achievable tumor-absorbed doses may consequently be suboptimal and impair treatment efficacy.

Moreover, tumor-absorbed dose quantification is scarce, and a clear dose–response relationship is lacking. Thus, effective tumor-absorbed dose values remain uncertain (reported range, 66–495 Gy) (*4*). Better definition of required absorbed tumor doses is crucial to assess whether the results of large comparative trials are the best that radioembolization has to offer before concluding its definitive role in the treatment of CRLM. Furthermore, establishing the dose–response relationship could stimulate the development of personalized methods for optimal prescribed activity calculation.

The purpose of this study was to assess the relationship between tumor-absorbed dose and response after resin microsphere ^{90}Y radioembolization in a prospective phase II clinical trial in patients with CRLM. Absorbed dose was quantified on posttreatment

Received Jan. 27, 2016; revision accepted Feb. 1, 2016.
For correspondence contact: Andor F. van den Hoven, Department of Radiology and Nuclear Medicine, University Medical Center Utrecht, Heidelberglaan 100, 3584 CX Utrecht, The Netherlands.
E-mail: a.f.vandenhoven@umcutrecht.nl
Published online Feb. 23, 2016.

^{90}Y PET, and response was measured by metabolic tumor response on ^{18}F-FDG PET.

MATERIALS AND METHODS

Study Design and Patient Selection

Between November 2011 and August 2014, a prospective, single-institution, phase II clinical trial (RADioembolization: Angiogenic factors and Response [RADAR] trial) was conducted. In this trial, 42 patients with unresectable, chemorefractory CRLM underwent resin ^{90}Y-microsphere (SIR-Spheres; SIRTeX) radioembolization. All patients were in good clinical condition (World Health Organization performance score < 2); had adequate liver, renal, and bone marrow functions; had a liver tumor burden $< 70\%$; and had no other contraindications for radioembolization. Workup and treatment protocol were in accordance with current standards of practice and are described in detail elsewhere (*5–7*). In brief, multimodality imaging (^{18}F-FDG PET, multiphasic liver CT, and liver MRI) and laboratory and clinical examinations were performed during workup. A week before treatment, patients underwent a standard preparatory angiography with the administration of ^{99m}Tc-labeled macroalbumin aggregates (^{99m}Tc-MAA). During treatment, radioactive ^{90}Y-microspheres were administered in the same catheter position. Pretreatment dosimetry was performed with the BSA method, as per the manufacturer's recommendation. With this method, prescribed activity is calculated in GBq by the following equation: BSA – 0.2 + fractional tumor burden. A bremsstrahlung SPECT/CT (in the first 10 patients) or ^{90}Y PET/CT ($n = 32$) was obtained after treatment. At 1-mo follow-up (1m FU) the ^{18}F-FDG PET scan and MRI of the liver were repeated for tumor response assessment. The medical ethics committee of the University Medical Center Utrecht approved this trial. Written informed consent was obtained from all patients before study entry.

For the current dose–response evaluation, only patients who were enrolled in the RADAR trial and who underwent an ^{18}F-FDG PET scan at our institution at baseline and 1m FU, as well as a postradioembolization ^{90}Y PET/CT, were included.

This study is reported according to the Strengthening the Reporting of Observational Studies in Epidemiology recommendations (*8*).

Dose–Response Evaluation

Tumor-absorbed dose and metabolic tumor response were assessed on ^{90}Y PET and ^{18}F-FDG PET, respectively, on a per-lesion basis and on a per-liver basis for the sum of all metastases.

All PET analyses were performed with ROVER software (ABX GmBH), which was developed for analysis of ^{18}F-FDG PET scans. Phantom experiments and clinical patient data were used to validate quantitative ^{90}Y PET analyses with this software (supplemental data [available at http://jnm.snmjournals.org]).

The relationship between radiation-absorbed dose and metabolic tumor response was evaluated with a regression model (see the "Statistical Analysis" section). For this purpose, individual metastases were automatically defined on the baseline ^{18}F-FDG PET scan in ROVER. An absolute threshold for activity concentration, based on the aortic blood-pool activity as recommended by the PET RECIST (threshold = 2 × mean SUV normalized for lean body mass [SUL_{mean}], measured in the aortic blood pool), and a volume restriction of 5 cm^3 or more were used to delineate solitary metastases with a metabolic activity exceeding the background activity of the healthy liver (*9*). Only regions with metabolic activity were delineated, thereby excluding non–PET-avid necrotic tumor cores. The resulting regions of interest were saved. For each tumor, metabolic activity was recorded as a partial-volume-corrected total lesion glycolysis (TLG*) value, which was determined by multiplying the metabolic tumor volume with its partial-volume-corrected SUL_{mean}.

This process was repeated for the 1m FU scan to assess the metabolic tumor response (change in TLG*) on a per-lesion basis. Care was taken to record baseline and FU values for the exact same lesions by reviewing the baseline and 1m FU images side by side. A TLG* value of 0 was appointed to lesions that were no longer identified at 1m FU, because the SUL_{mean} had fallen below the detection threshold. ROVER classified multiple lesions as 1 in the case of 1 hot voxel connection. Therefore, in cases in which separate baseline metastases appeared as fused at 1m FU, separate volumes were determined for the metastases on MRI of the liver at 1m FU and multiplied by the mean overall activity value of the fused metastasis to obtain separate TLG* values.

Next, baseline ^{18}F-FDG PET and ^{90}Y PET volumes were loaded into ROVER and coregistered on the basis of their low-dose CTs, using a built-in rigid transformation algorithm. The saved tumor regions of interest were automatically transferred to the ^{90}Y PET volumes after overlaying on the coregistered ^{18}F-FDG PET volume, enabling recovered activity calculations in Bq/mL for each metastasis (Fig. 1).

A correction factor (branching ratio (*10*)) was then applied to this recovered activity to adjust for the difference in specific positron branching fraction between the isotope selected in the scanner settings (β_x, in our case ^{89}Zr = 0.2275) and ^{90}Y ($\beta^{90}{}_Y = 31.86 \times 10^{-6}$):

$$\text{Corrected activity} = \left(\frac{\text{recovered activity}}{\beta_{90Y}}\right) \times \beta_X.$$

The corrected activity at the time of ^{90}Y PET acquisition was recalculated to the corrected activity at the time of treatment by adjustment for the radioactive decay. Consequently, tumor-absorbed doses were calculated as follows:

$$\text{Tumor-absorbed dose (Gy)} = \frac{(50\ \text{Gy} \times \text{Kg/GBq}) \times (\text{corrected activity in GBq})}{(\text{region-of-interest volume in mL} \times 1.06\ \text{g/mL})/1,000}.$$

Liver tumor dose (i.e., tumor-absorbed dose averaged over all liver metastases) was determined in a similar fashion, using the summed

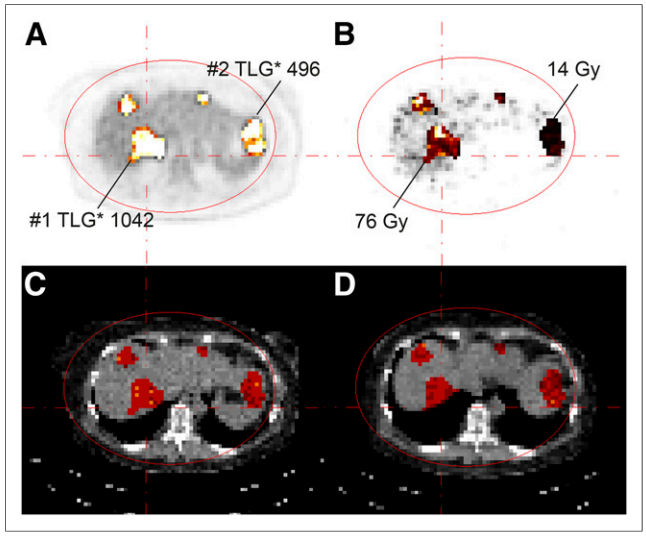

FIGURE 1. Example of quantitative PET analyses in ROVER. (A) Baseline ^{18}F-FDG PET scan was used to delineate multiple metastases and determine the TLG* per metastasis (e.g., 1, 1,042; 2, 496). (B) ^{90}Y PET scan was used to determine tumor-absorbed dose on a per-lesion basis (1, 76 Gy; 2, 14 Gy). Metastasis 1 in right hemiliver showed complete metabolic response at 1 mo after treatment, whereas residual metabolic activity was present in exophytic growing metastasis 2 in segment 2. (C and D) Low-dose CTs of the PET scans were used for image registration.

corrected activity and region-of-interest volume for all liver metastases within a patient's liver to fill in the former equation. Total liver dose (i.e., total absorbed dose in the entire treated liver) was determined using the net administered activity—calculated by dose calibrator measurements of the activity not injected—and the treated liver volume. The (first) treated liver lobe was included in the analysis in patients who received treatment of only a single lobe, or sequential treatment of both lobes.

Scanner Equipment, Acquisition, and Image Reconstructions

All PET/CT images were acquired on a Biograph mCT time-of-flight PET/CT scanner with TrueV (Siemens Healthcare). Our acquisition protocol for ^{18}F-FDG PET scans has been published elsewhere and includes daily quality controls (*11*). The PET/CT scans for ^{90}Y PET quantification were obtained on the day of treatment or the day after. This acquisition protocol consisted of two 20-min bed positions. Images were reconstructed with an iterative reconstruction algorithm, containing point spread function model and time-of-flight information, using 4 iterations with 21 subsets and a Gaussian post-reconstruction filter of 5 mm in full width at half maximum. A model-based scatter-correction method was used. Reconstructed voxel size was $2 \times 2 \times 2$ cm^3. A low-dose CT was acquired for attenuation correction, using an effective tube current time product of 40 mAs per rotation, an effective tube potential of 120 kV, and a slice thickness of 3 mm.

Statistical Analysis

Descriptive analyses were performed to summarize patient demographics, treatment characteristics, and TLG* and radiation-absorbed dose values.

A linear mixed-effects regression (LMER) model was fitted to evaluate the relationship between tumor-absorbed dose and posttreatment TLG* at 1m FU, adjusted for baseline TLG*, on a per-lesion basis. A more detailed explanation of this method can be found in the supplemental data.

Metabolic tumor and liver response were defined as a 50% or more decrease in TLG* at 1m FU for a metastasis or the sum of all liver metastases in a patient, respectively.

Univariable survival analysis was used to compare estimates in median overall survival (OS) between patients with and without metabolic liver response as well as average liver tumor dose $>$ 60 Gy and $<$ 60 Gy. OS was defined as the interval between treatment and death or last contact (date of censoring).

All analyses were performed with R version 3.1.2 (The R Foundation). A 2-sided P value < 0.05 was considered statistically significant.

RESULTS

Patient Demographics and Treatment Characteristics

Twelve of 42 patients were excluded for the following reasons: no postradioembolization ^{90}Y PET/CT ($n = 10$), baseline ^{18}F-FDG PET/CT not obtained at our institute ($n = 1$), and no ^{18}F-FDG PET/CT at 1m FU ($n = 1$).

Baseline characteristics of the 30 included patients are summarized in Table 1. Mean prescribed ^{90}Y activity was 1,827 ± 294 MBq. In 2 patients (7%), reduction in prescribed activity was necessary because of a liver-to-lung shunt fraction $>$ 10%. Whole-liver treatment was performed in 25 patients (83%). Only a single lobe was treated in 3 patients (10%), and 2 patients (7%) were treated with a sequential lobar approach. The mean net administered ^{90}Y activity was 1,751 ± 331 MBq, corresponding to a mean total liver dose of 50 ± 20 Gy (range, 18–109 Gy).

Tumor Dose and Metabolic Tumor Response

A total of 113 metastases were delineated, with a median number of 3 metastases per patient (range, 1–9). The mean tumor-absorbed dose was 51 ± 28 Gy (range, 7–174 Gy [Table 2]). In 28 patients (93%), tumor-absorbed dose exceeded 10 Gy in all metastases; this was 21 (70%) for $>$ 20 Gy, 14 (47%) for $>$ 30 Gy, 6 (20%) for $>$ 40 Gy, 3 (10%) for $>$ 50 Gy, and 1 (3%) for $>$ 60 Gy. Fifty-two of 113 metastases (46%) had a metabolic tumor response.

Mean liver tumor dose (averaged over all metastases per patient) was 57 ± 26 Gy (range, 18–109 Gy), corresponding to a mean tumor–to–total-liver dose ratio of 1.3 ± 0.6 (range, 0.5–3.2). Eleven of 30 patients (37%) had a metabolic liver response.

TABLE 1
Baseline Characteristics (30 Patients)

Characteristic	*n* or mean ± SD
Sex	
Male	19 (63%)
Female	11 (37%)
Age (y)	63 ± 12
Liver metastases	
Synchronous	24 (80%)
Metachronous	6 (20%)
World Health Organization performance status	
0	16 (53%)
1	13 (43%)
2	1 (3%)
Previous systemic therapy lines	
0	0 (0%)
1	12 (40%)
2	11 (37%)
>2	7 (23%)
Received bevacizumab	
Yes	17 (57%)
No	13 (43%)
Extrahepatic disease before treatment	
Yes	10 (33%)
Lymph node	5
Lung	2
Bone	3
Recurrence (colon/rectum)	3
Other	4
No	20 (67%)
Tumor burden (% of whole liver)	
<25%	27 (90%)
25%–50%	3 (10%)
>50	0
Metabolic tumor volume (mL)	301 ± 248

Data in parentheses are percentages. Metabolic tumor volume is total volume of metastases as delineated on ^{18}F-FDG PET at baseline.

TABLE 2
Tumor-Absorbed Dose and Metabolic Tumor Response

Baseline/outcome measure	Individual metastases (n = 113)	Sum of all metastases within liver (n = 30)
Mean tumor-absorbed dose ± SD	51 ± 28 Gy (range, 7–174)	57 ± 26 Gy (range, 18–109)
Median baseline TLG*	177 (range, 28–5,891; IQR, 459)	1350 (range, 181–5,891; IQR, 2,212)
Posttreatment TLG* at 1m FU	115 (range, 0–7,111; IQR, 478)	1,016 (range, 0–7,341; IQR, 2,786)
Metabolic response rate	52/113 (46%)	11/30 (37%)

Tumor-absorbed dose and metabolic tumor response results on level of individual metastases (n = 113) and for sum of all metastases per liver (n = 30). Data are mean ± SD, with range in parentheses; median, with range and interquartile range (IQR) in parentheses; or n, with percentages in parentheses.

Dose–Response Relationship

The relation between tumor-absorbed dose, baseline TLG*, and posttreatment TLG* was best explained by an LMER model using a linear function of dose, a quadratic function of baseline TLG*, and a logarithmic transformation of posttreatment TLG* (log [1m FU TLG* + 8]).

A strong and statistically significant dose–response relationship was found, with the dose effect depending on baseline TLG* (Table 3; Fig. 2). Increasing tumor-absorbed dose values were associated with better metabolic tumor response (decreased posttreatment TLG*, Fig. 2A) and metastases with high baseline TLG* required higher tumor-absorbed doses to show a reduction in metabolic activity than metastases with lower baseline TLG* (Fig. 2B). By conservative estimation, at least 40–60 Gy are required to induce a 50% reduction in TLG* for a metastasis with an average baseline TLG* value.

The model with and without the random patient-level intercept explained 78% and 56% of the variation in 1m FU TLG*, respectively.

Rerunning the analysis without the fused lesions or without truncation of baseline TLG* values did not diminish the dose-response relationship.

Exploratory Survival Analysis

The median OS was 9.4 mo (95% confidence interval [CI], 5.4–11.8 mo). Exploratory survival analysis suggested a significant association between metabolic liver response and OS (log-rank test, P = 0.02). The estimated median OS time was 11.6 mo (95% CI, 11.51–∞; n = 11) and 6.6 mo (95% CI, 4.8–11.7; n = 19) in patients with and without metabolic liver response, respectively (Fig. 3A). The median TLG* was 987 (range, 256–3,374) at baseline and 240 (range, 0–1,185) at 1 m after treatment for responders. In the nonresponders, median TLG* was 2,266 (range, 181–5,891) at baseline and 2,892 (range, 104–7,341) at 1 m after treatment. Patients with an average liver tumor dose > 60 Gy showed a trend (P = 0.05) of longer median OS (Fig. 3B): 5.3 mo (95% CI, 4.4–14.3; n = 18) versus 11.5 mo (95% CI, 10.6–∞; n = 12).

DISCUSSION

To our knowledge, this prospective study is the first to report a dose–response relationship in patients with CRLM treated with ^{90}Y radioembolization. With the currently used methods for activity prescription, tumor-absorbed doses were unexpectedly low and showed a strong intrapatient heterogeneity. Our results show that metastases with a higher tumor-absorbed dose have a better metabolic tumor response at 1 mo after treatment, a relation that was more pronounced in metastases with a high baseline metabolic activity. Furthermore, metabolic liver response was associated with prolonged OS, which further supports the idea that tumor-absorbed dose optimization improves patient outcome.

The success of radioembolization as a salvage treatment for patients with CRLM and other tumor types has brought investigations to a critical point. Now, several large, multicenter randomized controlled trials are investigating the benefit of adding radioembolization treatment to systemic therapy in the first- and second-line treatment of CRLM (*12*). These trials have the potential to define the role of radioembolization in the treatment paradigm for CRLM.

The results of our study are critical for a well-informed interpretation of these trials. For one, prescribed activity calculation methods are not yet optimized. The BSA method, used for radioembolization with resin ^{90}Y-microspheres, does not account for liver mass or expected intrahepatic microsphere distribution. The monocompartmental medical internal radiation dosimetry method, recommended for the use of glass ^{90}Y-microspheres, is only slightly more patient-specific; it incorporates a target dose for the entire liver and adjusts for the liver mass. Yet, interpatient variability is neglected with both methods, as if radioembolization were a 1-size-fits-all treatment.

The results of our study prove this assumption to be false. A true heterogeneity in absorbed dose distribution exists, between and within patients. The large SD and wide ranges in tumor-absorbed doses that we have found on a per-lesion and per-liver basis illustrate this fact. Furthermore, tumor-absorbed doses observed in our study

TABLE 3
Summary of LMER Model for TLG* at 1 Month After Treatment as Function of Tumor-Absorbed Dose and Baseline TLG*

Fixed effects	Direction of association	P
Tumor-absorbed dose	Negative	1.9×10^{-7}
Baseline TLG*	Positive	2.2×10^{-16}
Interaction (dose:baseline TLG*)	Negative	1.4×10^{-3}

This table summarizes the most important findings of the LMER model. Direction of association is shown in this table, instead of regression coefficients, to simplify interpretation of this complex model. Negative direction of association for tumor-absorbed dose, for example, indicates negative regression coefficient, meaning that increased tumor-absorbed dose is associated with decreased posttreatment TLG*. Exact P values are given for fixed effects.

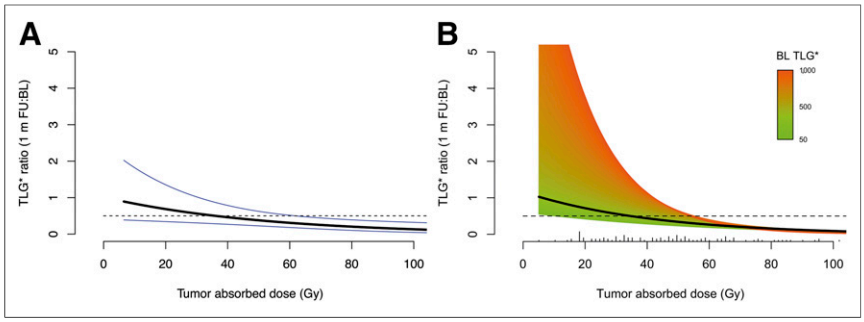

FIGURE 2. Dose–response curves estimated by LMER model. (A) Illustration of relationship between tumor-absorbed dose (*x*-axis) and metabolic tumor response (*y*-axis, 1m FU TLG*: baseline TLG*) for a metastases with a mean baseline TLG* value (black line). Blue lines indicate associated 95% CI bands. By conservative estimation, at least 40–60 Gy is required for a 50% TLG* reduction (intersection of black line and upper 95% CI line with dotted reference line). (B) Added color grading in this illustration indicates how the dose–response curve differs for other levels of baseline TLG* (increasing from green to orange and red). With increasing absorbed dose, metabolic tumor response is more likely, but with increasing baseline TLG* (i.e., color grading) tumor response is less likely. Metastases with high baseline TLG* value need to absorb higher radiation dose to achieve same metabolic tumor response as metastases with lower baseline TLG*.

were relatively low; only 20% of patients had a tumor-absorbed dose > 40 Gy in all metastases, whereas the dose–response curve indicated 40–60 Gy as effective values for average metastases. Current pretreatment ^{90}Y activity calculations curb the maximum tolerable healthy liver tissue dose. As a consequence, a metabolic tumor response was achieved in less than half of metastases and metabolic liver response in only one third of patients. Although the patients in our trial were heavily pretreated salvage patients, this seems insufficient.

Thus, a more personalized approach to radioembolization is needed to optimize tumor dose delivery in patients with CRLM. This requires several changes to the current treatment paradigm. Using a scout dose of radioactive microspheres during the preparatory angiography may prove better suited to predict the therapeutic microsphere distribution than ^{99m}Tc-MAA (*13*). Once the therapeutic microsphere distribution can be predicted, pretreatment activity calculation can be tailored to the individual patient with the previously described artery-specific partition model, yielding a distribution-specific maximum tolerable treatment activity (*14*). Furthermore, different strategies may improve tumor targeting during the treatment procedure itself, including the use of a vasoconstrictor or another catheter type to affect hemodynamics (*15,16*). A better understanding of the dose–response relationship also creates a framework for the measurement of technical success after treatment, both in clinical practice and in research. If, for example, posttreatment ^{90}Y PET demonstrates a subtherapeutic tumor-absorbed dose in a metastasis in clinical practice, additional treatment with another therapeutic modality or selective retreatment with radioembolization may be considered. In a research setting, investigators should implement in vivo dose quantification into their study protocol and report tumor-absorbed dose data. This may help interpreters to distinguish between suboptimal tumor response rates due to technical failure or refractory disease.

Interestingly, we found that the dose effect is dependent on the baseline TLG*. To the best of our knowledge, this has not been reported before. With increasing tumor volume, a homogeneous ^{90}Y-microsphere distribution in the tumor compartment becomes less likely, so a high tumor-absorbed dose may be required in metastases with a high baseline TLG* to ensure a minimum dose throughout the entire tumor. In addition, the aggressive nature of metastases with a high baseline TLG* may render these tumors less likely to respond to therapy. The dependency of the dose effect on baseline metabolic activity suggests that 1 threshold for an effective tumor-absorbed dose after radioembolization may be too simplistic. Further research has to show whether our range of effective tumor-absorbed dose values as a function of baseline metabolic activity can be further refined.

Distinctive strengths of our investigation include the prospective study design that ensures standardization of study procedures, the per-lesion basis analyses, the use of an LMER model that accounts for data clustering, actual quantitative absorbed dose measurements on ^{90}Y PET, and the use of objective metabolic tumor response parameters based on ^{18}F-FDG PET.

Previous studies have reported retrospective data to support a dose–response association for radioembolization treatment but failed to uncover the nature of this relationship in patients with CRLM (*17–20*). Most other dose–response evaluations in radioembolization studies either focused on hepatocellular carcinoma or used glass ^{90}Y-microspheres. The dose–response associations derived from these studies are, however, not directly comparable to our findings. For one, radiosensitivity may be dependent on tumor type, similar to findings in external-beam radiotherapy (*21*). Furthermore, tumor-absorbed dose values are generally higher with glass microspheres, but this does not necessarily imply greater treatment efficacy. This may be attributed to the fact that glass microspheres are injected in lower numbers but with much higher specific activity per sphere. Furthermore, treatment with resin microspheres likely results in a combined

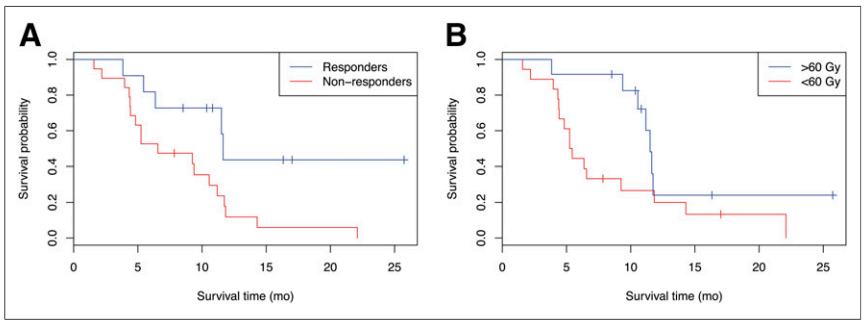

FIGURE 3. Survival curves stratified on metabolic liver response and average liver tumor dose. (A) Patients with (blue line) metabolic liver response (50% decrease in TLG* at 1 mo after treatment) showed significantly longer median OS than nonresponders (red line). (B) Patients with average liver tumor dose exceeding 60 Gy (blue line) showed trend of longer median OS than those with lower liver tumor dose (red line).

embolic and radiation effect, whereas glass microspheres rely much more on radiation alone.

Our study has several limitations. First, the number of study patients was limited, and substantial interpatient heterogeneity existed despite similar tumor types and disease stages. Therefore, the variation explained by the LMER model heavily depended on the random intercept. Consequently, our model's ability to predict metabolic tumor response on the basis of tumor-absorbed dose may be limited in an external dataset. Furthermore, it seems reasonable to assume that the observed tumor response is a consequence of absorbed radiation doses, because all patients had confirmed progressive disease at the time of inclusion in our study, no competing therapies were given, and we adjusted for baseline TLG*, which contains information about the volume and metabolic activity of individual metastases. Nonetheless, we cannot rule out potential confounding by tumor biology. Second, we measured only tumor response at 1m FU. Third, because the found dose–response relationship was specific for resin ^{90}Y-microsphere radioembolization in salvage patients with CRLM, validation in other disease stages, tumor types, and type of microspheres is required. Fourth, the generalizability of TLG* values is limited. They are not a biologic constant but depend on the use of specific hardware, image acquisition, and reconstruction protocol and image analysis software for ^{18}F-FDG PET scans. Fifth, the coregistration of the baseline ^{18}F-FDG PET and ^{90}Y PET images was challenging, and small registration errors are currently unavoidable.

With the increasing application of radioembolization as a treatment for CRLM, and a gradual shift toward earlier disease stages, it is of paramount importance to critically reflect on the current status of this technique and acknowledge aspects that are in need for optimization. These aspects need to be improved to enable a personalized approach to radioembolization that aims for maximum treatment efficacy while respecting safety concerns. The limitations of current radioembolization practice should also be considered when interpreting the results of large randomized controlled trials.

CONCLUSION

A strong dose–response relationship exists for the treatment of CRLM with resin microsphere ^{90}Y radioembolization. Treatment efficacy is, however, still limited, because the currently used pretreatment activity calculation methods curb potentially achievable tumor-absorbed dose values. A more personalized approach to radioembolization is required before concluding on its clinical potential.

DISCLOSURE

The costs of publication of this article were defrayed in part by the payment of page charges. Therefore, and solely to indicate this fact, this article is hereby marked "advertisement" in accordance with 18 USC section 1734. Miriam Koopman is advisor for Amgen, Bayer Healthcare, Merck, Nordic Pharma, and Roche. Marnix G.E.H. Lam is advisor for BTG and Bayer Healthcare and speaker for Sirtex Medical Inc. The Department of Radiology and Nuclear Medicine of the University Medical Center Utrecht has received royalties by Quirem Medical. No other potential conflict of interest relevant to this article was reported.

REFERENCES

1. Kennedy A. Radioembolization of hepatic tumors. *J Gastrointest Oncol.* 2014;5: 178–189.
2. Rosenbaum CENM, Verkooijen HM, Lam MGEH, et al. Radioembolization for treatment of salvage patients with colorectal cancer liver metastases: a systematic review. *J Nucl Med.* 2013;54:1890–1895.
3. Dutton SJ, Kenealy N, Love SB, Wasan HS, Sharma RA. FOXFIRE protocol: an open-label, randomised, phase III trial of 5-fluorouracil, oxaliplatin and folinic acid (OxMdG) with or without interventional selective internal radiation therapy (SIRT) as first-line treatment for patients with unresectable liver-only or liver-dominant metastatic colorectal cancer. *BMC Cancer.* 2014;14:497.
4. Cremonesi M, Chiesa C, Strigari L, et al. Radioembolization of hepatic lesions from a radiobiology and dosimetric perspective. *Front Oncol.* 2014;4:210.
5. Mahnken AH, Spreafico C, Maleux G, Helmberger T, Jakobs TF. Standards of practice in transarterial radioembolization. *Cardiovasc Intervent Radiol.* 2013;36: 613–622.
6. Giammarile F, Bodei L, Chiesa C, et al. EANM procedure guideline for the treatment of liver cancer and liver metastases with intra-arterial radioactive compounds. *Eur J Nucl Med Mol Imaging.* 2011;38:1393–1406.
7. van den Hoven AF, Smits MLJ, de Keizer B, van Leeuwen MS, van den Bosch MAAJ, Lam MGEH. Identifying aberrant hepatic arteries prior to intra-arterial radioembolization. *Cardiovasc Intervent Radiol.* 2014;37:1482–1493.
8. von Elm E, Altman DG, Egger M, Pocock SJ, Gøtzsche PC, Vandenbroucke JP. The strengthening the reporting of observational studies in epidemiology (STROBE) statement: guidelines for reporting observational studies. *J Clin Epidemiol.* 2008;61:344–349.
9. Wahl RL, Jacene H, Kasamon Y, Lodge MA. From RECIST to PERCIST: evolving considerations for PET response criteria in solid tumors. *J Nucl Med.* 2009;50(suppl 1):122S–150S.
10. Pasciak AS, Bourgeois AC, Bradley YC. A comparison of techniques for ^{90}Y PET/CT image-based dosimetry following radioembolization with resin microspheres. *Front Oncol.* 2014;4:121.
11. Rosenbaum CENM, van den Bosch MAAJ, Veldhuis WB, Huijbregts JE, Koopman M, Lam MGEH. Added value of FDG-PET imaging in the diagnostic workup for yttrium-90 radioembolisation in patients with colorectal cancer liver metastases. *Eur Radiol.* 2013;23:931–937.
12. Braat AJAT, Smits MLJ, Braat MNGJA, et al. ^{90}Y hepatic radioembolization: an update on current practice and recent developments. *J Nucl Med.* 2015;56:1079–1087.
13. Prince JF, van Rooij R, Bol GH, de Jong HWAM, van den Bosch MAAJ, Lam MGEH. Safety of a scout dose preceding hepatic radioembolization with ^{166}Ho microspheres. *J Nucl Med.* 2015;56:817–823.
14. Kao YH, Hock Tan AE, Burgmans MC, et al. Image-guided personalized predictive dosimetry by artery-specific SPECT/CT partition modeling for safe and effective ^{90}Y radioembolization. *J Nucl Med.* 2012;53:559–566.
15. van den Hoven AF, Smits MLJ, Rosenbaum CENM, Verkooijen HM, van den Bosch MAAJ, Lam MGEH. The effect of intra-arterial angiotensin II on the hepatic tumor to non-tumor blood flow ratio for radioembolization: a systematic review. *PLoS One.* 2014;9:e86394.
16. Pasciak AS, Mcelmurray JH, Bourgeois AC, Heidel RE, Bradley YC. The impact of an antireflux catheter on target volume particulate distribution in liver-directed embolotherapy: a pilot study. *J Vasc Interv Radiol.* 2015;26:660–669.
17. Flamen P, Vanderlinden B, Delatte P, et al. Multimodality imaging can predict the metabolic response of unresectable colorectal liver metastases to radioembolization therapy with yttrium-90 labeled resin microspheres. *Phys Med Biol.* 2008;53:6591–6603.
18. Lam MGEH, Goris ML, Iagaru AH, Mittra ES, Louie JD, Sze DY. Prognostic utility of ^{90}Y radioembolization dosimetry based on fusion ^{99m}Tc-macroaggregated albumin-^{99m}Tc-sulfur colloid SPECT. *J Nucl Med.* 2013;54:2055–2061.
19. Lam MGEH, Banerjee A, Goris ML, et al. Fusion dual-tracer SPECT-based hepatic dosimetry predicts outcome after radioembolization for a wide range of tumour cell types. *Eur J Nucl Med Mol Imaging.* 2015;42:1192–1201.
20. Demirelli S, Erkilic M, Oner AO, et al. Evaluation of factors affecting tumor response and survival in patients with primary and metastatic liver cancer treated with microspheres. *Nucl Med Commun.* 2015;36:340–349.
21. Lausch A, Sinclair K, Lock M, et al. Determination and comparison of radiotherapy dose responses for hepatocellular carcinoma and metastatic colorectal liver tumours. *Br J Radiol.* 2013;86:20130147.